THE JOURNAL OF PHYSICAL CHEMISTRY C

Article

pubs.acs.org/JPCC

# Aggregation Kinetics and Stability Mechanisms of Pristine and Oxidized Nanocarbons in Polar Solvents

Nima Sefidmooye Azar[†] and Mahdi Pourfath*[,†,‡,§]

[†]School of Electrical and Computer Engineering, University of Tehran, P.O. Box: 14395-515, Tehran, Iran

[‡]School of Nano Science, Institute for Research on Fundamental Sciences (IPM), P.O. Box 19395-5531, Tehran, Iran

[§]Institute for Microelectronics, Technische Universität Wien, Vienna 1040, Austria

Supporting Information

**ABSTRACT:** Owing to their high propensity for bundling and aggregation, effective and stable dispersion of nanocarbons in polar solvents is of key significance in the preparation of carbon nanotube (CNT) and graphene nanosheet (GNS)-based devices and nanocomposites. Previous studies have shown that oxidation of CNT side walls and GNS surfaces ameliorates their stability in polar solvents. In this study, large-scale all-atom molecular dynamics simulations were employed to shed light on the stability mechanisms of nanocarbons in polar solvents and explicate the role of surface modification in their dispersibility enhancement. The concepts of potential of mean force (PMF) and translational kinetic energy (TKE) were utilized for this purpose. Our studies disclosed the physical facts lying behind the remarkably higher stability of modified nanocarbons in polar solvents compared to the pristine ones. First, the oxidized nanocarbons are intrinsically much less motivated to form aggregates, and second, the solvent-induced repulsion is much stronger in the case of oxidized nanocarbons. It was also revealed that among the various solvents considered here, *N*-methyl-2-pyrrolidone (NMP) provides the most stable solutions for the both pristine and oxidized nanocarbons, followed by dimethyl sulfoxide (DMSO), dimethylformamide (DMF), 1,2-dichlorobenzene (ODCB), and tetrahydrofuran (THF). This work provides a comprehensive understanding of the nanocarbons stability that will facilitate the handling of their aggregation issue.

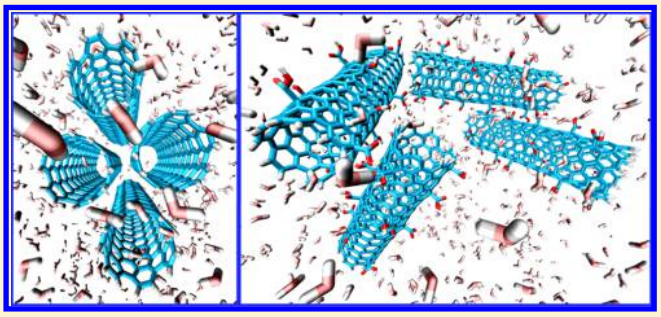

## INTRODUCTION

Due to their extraordinary electrical,[1] optical,[2] and chemical[3] properties, such as high electron mobility, tunable direct band gap, and high surface-to-volume ratio, carbon nanotubes (CNTs) and graphene nanosheets (GNSs) are recognized as promising candidates for future electronic, optoelectronic, and sensing applications.[4] Furthermore, the relatively high electrical[1] and thermal[5] conductivity and superior mechanical flexibility and strength[4] render them favorable fillers for reinforcing polymers[6] to obtain functional nanocomposites,[7] such as highly stretchable, transparent[8] conducting films[9] and electromagnetic interference shielding layers.[6,10,11] One major obstacle for realizing the potentials of carbon-based nanostructures is their great inclination to aggregate[12] and form bundles,[13] which arises from high hydrophobicity and the strong van der Waals attractions.[14]

Functionalizing CNTs and GNSs is the widespread solution to their dispersion issue in polar solvents,[15] which mainly includes noncovalent dispersion[16] using surfactants[17] and polymers[18] and covalent modification of the surface.[19,20] The latter, which is to attach functional groups to the side walls and open ends of the nanocarbons,[21] is known as an efficient method for dispersing nanocarbons.[22] The most common and primary surface modification approach toward solubilizing CNTs and GNSs in polar solvents is oxidizing the nanocarbons through nitric acid treatment.[23−25] This treatment leaves the nanocarbons with oxygen-containing functional groups such as carboxyl (−COOH) and hydroxyl (−OH) groups[26,27] and results in highly stable nanocarbons in water and other polar solvents.[28] Yet it leads to the degradation of CNTs and GNSs intrinsic qualities by introducing structural defects.[29] Still, some studies suggested that by carefully choosing the treatment conditions one can obtain highly dispersible nanocarbons with acceptable characteristics.[30,31]

Recently, molecular dynamics (MD) simulations have been broadly utilized to study the dispersion and stabilization of CNTs and GNSs in aqueous environments.[32] Most of these studies focused on the stabilization of nanocarbons using noncovalent techniques.[33,34] One useful MD concept for studying the dispersion of nanostructures in different media is that of the potential of mean force (PMF).[35,36] PMF profiles provide valuable insights into the nanocarbons resistance against exfoliation, tendency to bundle after separation, and solvent-induced interactions against their agglomeration. Choudhury et al.[37] studied the stability of pristine graphene nanosheets in water by deriving the PMF curves. By utilizing a

**Received:** May 26, 2016
**Revised:** June 30, 2016
**Published:** July 14, 2016





DOI: 10.1021/acs.jpcc.6b05318
J. Phys. Chem. C 2016, 120, 16804−16814

similar approach, Xu et al.[35] investigated sodium dodecyl sulfate-assisted dispersions of single-wall CNTs in water. Other studies using PMF include investigating the dispersion properties of boron-doped CNTs in water solution,[38] stability of fullerene $C_{60}$ in ethanol solution,[39] and effect of the amphiphilic coatings on the stability of CNTs in aqueous solutions.[40]

In the present work, we employed large-scale all-atom molecular dynamics simulations in order to study the stability of pristine, carboxylated, and hydroxylated single-wall carbon nanotubes (CNT) and single-layer graphene nanosheets (GNS) in polar solvents including water, dimethylformamide (DMF), tetrahydrofuran (THF), *N*-methyl-2-pyrrolidone (NMP), chloroform, 1,2-dichlorobenzene (ODCB), dimethyl sulfoxide (DMSO), toluene, methanol, and acetone, which are the widely used solvents for the exfoliation of graphene[12] and preparation of CNT solutions.[41] Carboxyl (−COOH) and hydroxyl (−OH) functional groups with a degree of 5% were attached to pristine CNT and GNS in order to evaluate the effect of surface oxidation on the dispersion of nanocarbons in various solutions. The PMF acting between pristine and functionalized nanocarbons were calculated to determine the solvent-induced potential barriers against their aggregation and the van der Waals (vdW) potential traps. Furthermore, the concept of PMF was accompanied by that of the translational (as opposed to rotational) kinetic energy (TKE) which provides a deeper understanding of the dispersion phenomenon. The dispersibility of nanocarbons was also studied by performing a set of larger scale free (unconstrained) MD simulations which revealed further facts on the aggregation and stability mechanisms of the nanocarbons. The systematic approach toward the dispersion and aggregation phenomena, developed in this work, enables us to explain the high stability of oxidized nanocarbons in polar solvents and also benchmark the ability of various polar solvents to disperse pristine and oxidized nanocarbons.

## SIMULATION METHOD

We utilized the OPLS-AA[42,43] force field to model the bonded and van der Waals (vdW) interactions of the solvent molecules. The SPC/E model[44] was used for simulating the water molecules. For acetone, methanol, DMSO, and ODCB, the partial charges were taken from the OPLS-AA force field, which led to acceptable bulk density values. The partial charges for DMF, THF, NMP, chloroform, and toluene were obtained from density functional theory (DFT) calculations with B3LYP exchange-correlation functional and 6-311++G** basis set using the electrostatic potential (ESP) fitting method implemented in the NWChem 6.6[45] software package, and the results are illustrated in Figure S1 and Tables S1−S9 in the Supporting Information. The calculated bulk densities of solvents are in good consistency with experimental values[46] and are reported in Table 1.

A 3 nm long (6,6) armchair single-wall CNT and a graphene nanosheet obtained from unzipping the same CNT structure were considered in our studies. Carboxyl and hydroxyl functional groups, with a functionalization degree of 5%, were randomly attached to the surface of the carbon nanostructures to portray the chemically modified nanocarbons. After preparing the nanocarbons, their structures were optimized utilizing the self-consistent charge density functional tight binding (SCC-DFTB)[47] approach implemented in the DFTB+[48] code and using the mio-1-1 Slater−Koster parameters set.

**Table 1. Solvent Bulk Densities Calculated (calcd) in This Study Compared to the Experimental (exp.) Values Reported in Ref 46 (at 298.15 K and 1 bar)**

| | water | DMF | THF | NMP | chloroform |
|---|---|---|---|---|---|
| density (calcd) [g/mL] | 0.998 | 0.943 | 0.864 | 1.026 | 1.473 |
| density (exp.) [g/mL] | 0.997 | 0.945 | 0.883 | 1.023 | 1.479 |
| | ODCB | DMSO | toluene | methanol | acetone |
| density (calcd) [g/mL] | 1.283 | 1.103 | 0.856 | 0.777 | 0.798 |
| density (exp.) [g/mL] | 1.300 | 1.101 | 0.862 | 0.792 | 0.791 |

The Lennard−Jones (LJ) parameters as well as the parameters for bonded interactions including the stretching force constants of angles and dihedral potentials for the basal carbon atoms, end hydrogens, hydroxyl, and carboxyl functional groups were adopted from the OPLS-AA force field. These included aromatic ring, alcohol, and carboxylic acid parameters, respectively. The same set of parameters was successfully used by previous studies (only LJ or only bonded interactions in some cases) to model the interactions of pristine,[49,50] carboxylated, and hydroxylated[51,52] carbon nanostructures with other molecules. Bond lengths and bond angles of the carbon nanostructures were derived from the SCC-DFTB calculations. In order to avoid unnecessary emphasis on the finite size of the carbon nanostructures, all basal carbon atoms (except for the ones attached to the functional groups in the functionalized structures) as well as the end hydrogens were treated as uncharged atoms (see a discussion on this matter and partial charge calculation for oxidized nanocarbons in the Supporting Information). The partial charges on functional groups were calculated within the B3LYP/6-311++G** theory using the sample structures depicted in Figure S2 and the ESP method, and the results are illustrated in Figure S3 and Tables S10 and S11 in the Supporting Information. Figure 1 shows the relaxed configurations of the nanostructures investigated in this work.

All MD simulations were carried out using the GROMACS 5.1[53,54] software package, and the equations of motion were integrated using the leapfrog scheme with a 2 and 1 fs time step during the equilibration and production runs, respectively. We employed NPT ensemble (constant number of atoms, constant pressure $P$ = 1 bar, and constant temperature $T$ = 298.15 K) in all simulations. In the course of production runs, the pressure was coupled to an isotropic Parrinello−Rahman barostat[55] (with a time constant of 6 ps) and the temperature was regulated using the Nose−Hoover thermostat[56] (with a time constant of 0.4 ps). For equilibration purposes, a Berendsen barostat[57] (with a time constant of 2 ps) was implemented to keep the system at constant pressure. The LJ parameters for interactions between atoms of different kinds were derived from geometric averaging rules $\sigma_{ij} = (\sigma_{ii}\sigma_{jj})^{1/2}$ and $\epsilon_{ij} = (\epsilon_{ii}\epsilon_{jj})^{1/2}$. The LJ interactions were treated with a cutoff distance of 1 nm. Short-range electrostatic interactions, up to a distance of 1 nm between the interacting atoms, were directly calculated using the Coulomb law. The electrostatic interactions beyond 1 nm were accounted for employing the particle-mesh Ewald (PME) summation method.[58] Bond lengths were constrained using the LINCS algorithm[59] in all simulations. Periodic boundary conditions were applied in all three directions.

The PMF profiles were calculated by numerically integrating the time-averaged force acting to separate the nanocarbons, while they were held at various center-of-mass (COM) distances. To be more specific, the PMF as a function of the


DOI: 10.1021/acs.jpcc.6b05318
J. Phys. Chem. C 2016, 120, 16804−16814

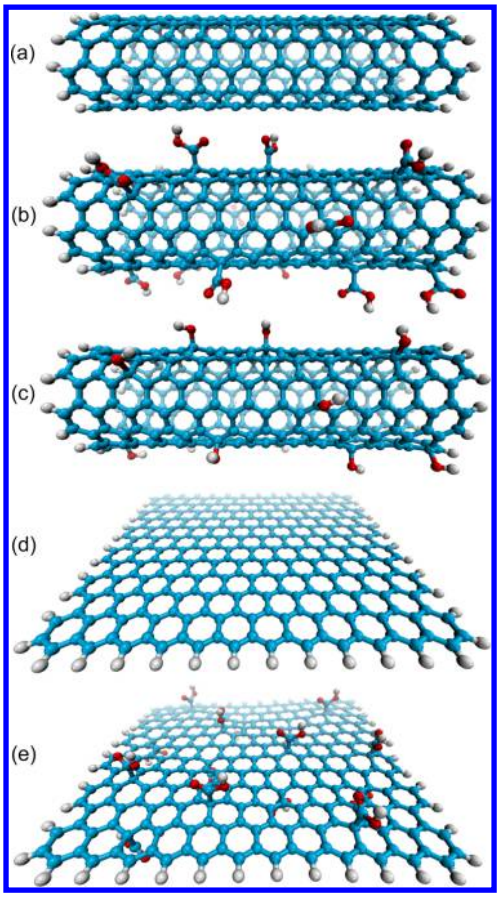


**Figure 1.** SCC-DFTB-optimized molecular structures of the nanocarbons considered in this study: (a) pristine 3 nm long (6,6) armchair single-wall carbon nanotube (CNTP), (b) 5% carboxylated CNT (CNTCOOH), (c) 5% hydroxylated CNT (CNTOH), (d) pristine single-layer graphene nanosheet obtained by unzipping the CNT structure (GNSP), and (e) 5% carboxylated graphene nanosheet (GNSCOOH). Each sphere represents an atom using the following color code: light blue, carbon; white, hydrogen; and red, oxygen.

COM distance ($d$) between the two nanostructures was calculated using the following relation[35,36,60]

$$\mathrm{PMF}(d) = \int_{d}^{d'} (\overrightarrow{F(\vec{r})}\cdot\hat{r})\mathrm{d}r \tag{1}$$

where $r$ is the same reaction coordinate as $d$, $d'$ is the COM distance where the PMF is set to zero (ranging from 1.5 to 2.5 nm depending on the structure of the nanocarbons), $\hat{r}$ is the unit vector along the direction connecting the COMs of the two nanocarbons, and $\vec{F}(\vec{r})$ is the constraining force exerted on one of the nanostructures from the opposing, position-restrained nanostructure (the reference nanocarbon) and the surrounding solvent molecules while the nanostructures are constrained at a COM distance of $r$ and restrained in a parallel configuration.

A series of successive constraint MD simulations was conducted to calculate a PMF curve. First, the two nanocarbons were located at a COM distance of $d'$ (where the PMF was assumed to be zero), and the simulation box was filled with the solvent molecules. The size of the simulation box was ~7 × 6 × 6 and ~7 × 7 × 4.5 nm$^3$ for CNT and GNS structures, respectively, and it was large enough along the reaction coordinate ($z$ direction here) to prevent the periodic images of the system from interfering with the force calculations. Then the simulation box was equilibrated for 10 ns while the solutes were severely restrained at their positions. Subsequently, the two nanocarbons were pulled slowly toward each other at a pace of 0.5 fm/ps using the constraint pulling algorithm implemented in the GROMACS software package. Afterward, ~50 configurations with an asymmetric spacing were extracted from the ~1.2 nm long pulling trajectory, which served as the initial configurations for the PMF calculations. Next, each configuration was equilibrated for 3 ns, and another 3 ns production run was then performed for PMF data collection, while the COM distance of the nanocarbons was constrained using the LINCS scheme. The trajectories and forces were saved every 4 ps during this course.

Translational kinetic energy of a nanostructure was calculated using the following relation

$$\mathrm{TKE} = \frac{1}{2}M(\overrightarrow{v_{\mathrm{com}}}\cdot\hat{r})^2 \tag{2}$$

where $M$ is the total mass of the nanostructure, $\vec{v}_{\mathrm{com}}$ is its center of mass velocity, and $\hat{r}$ is the same unit vector as that in PMF calculations. TKE calculation was performed after removing the distance constraint, while the reference nanocarbon was still position restrained.

## RESULTS AND DISCUSSION

**Interactions of Nanocarbons in Vacuum.** First, we studied the interactions of pristine and functionalized nanocarbons in the absence of the solvent molecules. PMF profiles of two opposing nanostructures in vacuum were calculated to this end, and the results are depicted in Figure 2a for the CNT and Figure 2b for GNS structures. To avoid exaggerating the

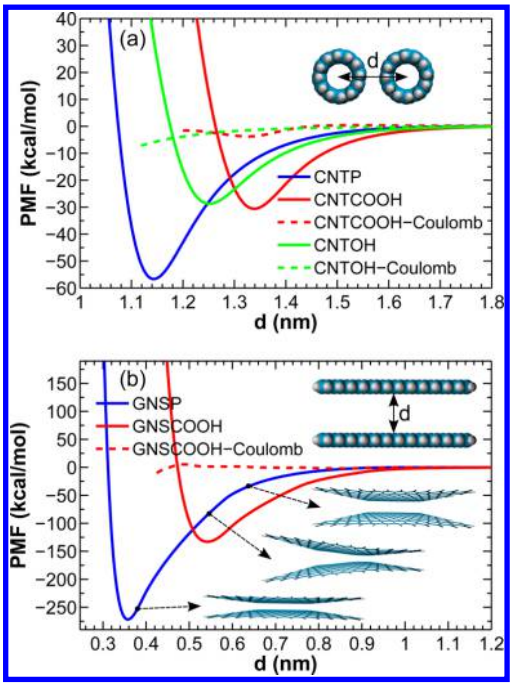


**Figure 2.** Potential of mean force profiles for two parallel nanostructures calculated in the absence of solvent molecules for (a) pristine, hydroxylated, and carboxylated CNTs and (b) pristine and carboxylated GNSs. $d$ is the COM distance between the nanocarbons. Coulombic component of the total PMF is also depicted. Some snapshots of the GNSP simulation trajectory are illustrated in the inset of b.



DOI: 10.1021/acs.jpcc.6b05318
J. Phys. Chem. C 2016, 120, 16804−16814

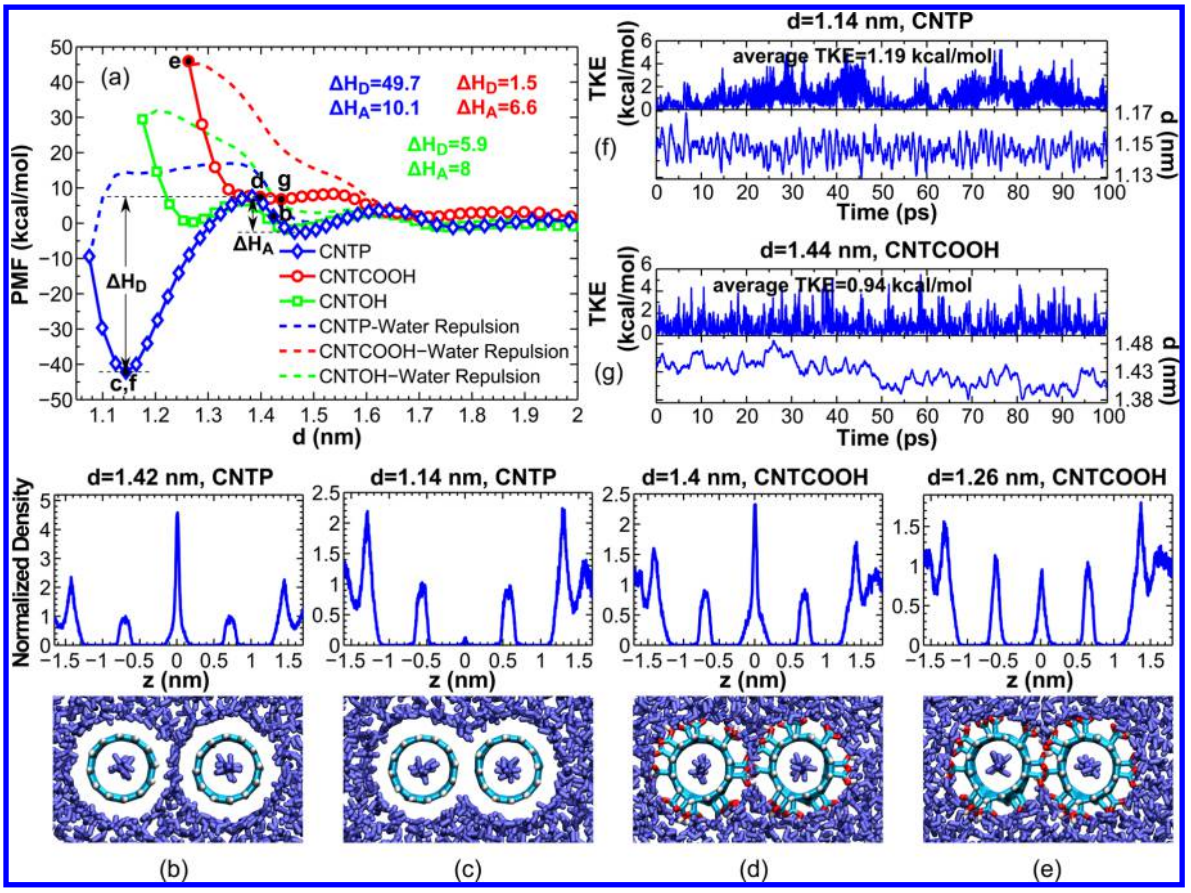


**Figure 3.** Set of simulations carried out for systems of pristine and oxidized CNTs in aqueous environment. (a) PMF profiles for pristine, hydroxylated, and carboxylated CNTs and the contribution from water repulsion to the total PMFs. $\Delta H_D$ and $\Delta H_A$ stand for the potential barrier height against dispersion and aggregation, respectively. (Inset) Calculated $\Delta H_D$ and $\Delta H_A$ values in kcal/mol. The points b, c, d, e, f, and g correspond to the parts b, c, d, e, f, and g, respectively. (b and c) Time-averaged normalized density profiles (density profiles normalized to the bulk density of water) along with snapshots of the simulation trajectory for pristine CNTs at two different COM distances. (d and e) Same as b and c for carboxylated CNTs. (f) Translational kinetic energy and displacement of a free nanostructure trapped in the potential well labeled by f on the PMF profile of pristine CNTs in part a in a time span of 100 ps. (Inset) Average value of TKE in this interval. (g) Same as f for carboxylated CNTs in the potential trap marked as g in part a.Color scheme for the snapshots included in parts b−e: light blue, carbon; white, hydrogen; red, oxygen; and dark blue, water molecules.

effect of surface modification on the dispersion properties, the functional groups were located on the basal carbon atoms in such a way that the functional atoms on the opposing nanocarbons did not meet directly as the nanocarbons approached each other. This can also be deduced from the little contribution of the Coulombic interactions to the total PMF profiles in Figure 2, considering the fact that only the functional atoms and the basal carbon atoms attached to them contained partial charges (as discussed in the previous section).

As illustrated in Figure 2, the oxidized nanocarbons manifest a much weaker tendency to aggregate in comparison with the pristine ones. This is concluded from the much shallower potential well of the oxidized nanocarbons whose depths are approximately one-half of the those of pristine nanostructures and can be explained considering the approaching LJ spheres. As the two oxidized nanocarbons get closer, at a COM distance which is 1.34 nm for CNTCOOH, 1.25 nm for CNTOH, and 0.54 nm for GNSCOOH, the functional atoms on one nanocarbon start to repel the basal carbon atoms on the opposing nanostructure which compensates for the increasing attraction between the basal carbon atoms on the two nanocarbons.

It should also be mentioned that the PMF profiles obtained for GNS structures here deviate from the ideal PMF profile of a set of LJ spheres approaching each other with constant structures. This stems from their structural properties and the fact that we employed realistic models (as opposed to the rigid structures used in some other studies[38,61]) and the GNSs bend at some points along the PMF profile (see the inset of Figure 2b). For CNTs, such behavior was not observed even though the same molecular models were employed for CNTs and GNSs, as comprehensively discussed in the previous section.

**Interactions of Nanocarbons in Solvent Media.** In addition to the major potential trap which results from the strongly attractive LJ interactions of the carbon atoms and is accountable for the CNT bundling and GNS stacking, the PMF profile of a pristine nanostructure in the presence of solvent molecules is characterized by several repulsion peaks and minor attraction traps.

Figure 3 presents the results obtained from a set of simulations performed for systems of pristine and oxidized CNTs in aqueous environment. As depicted in Figure 3a and already discussed, the PMF profile for pristine CNT features several potential traps and barriers. The deepest potential well at a COM distance of 1.14 nm is constructed by the strong LJ


DOI: 10.1021/acs.jpcc.6b05318
J. Phys. Chem. C 2016, 120, 16804−16814

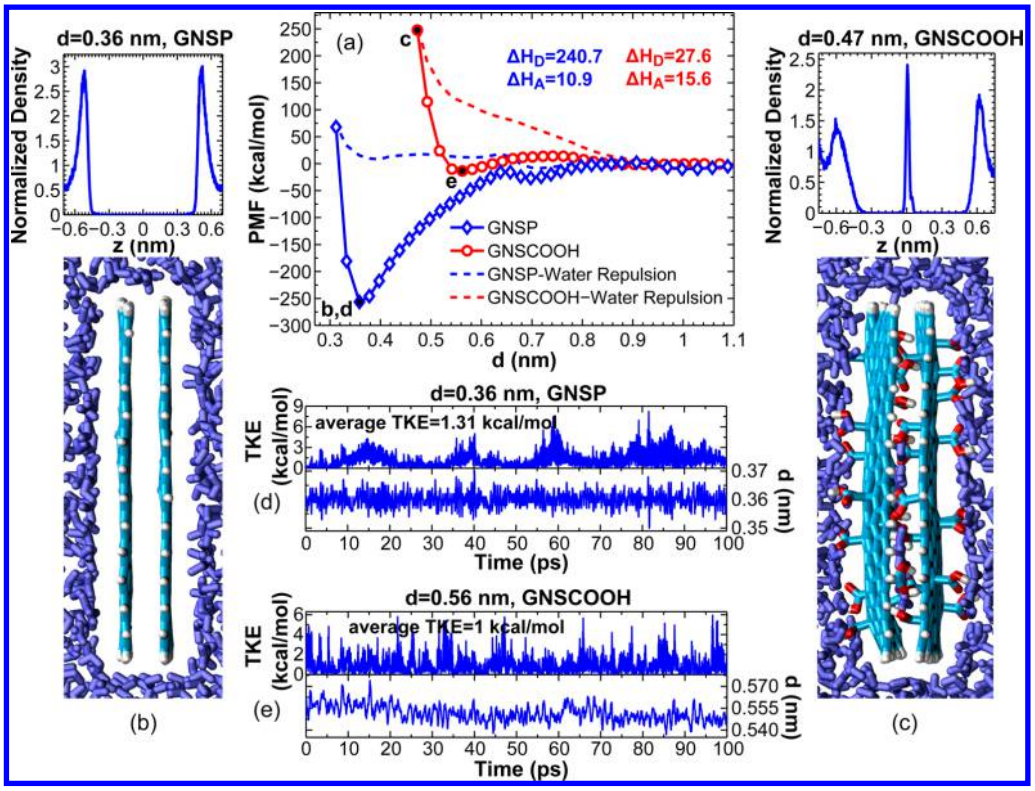


**Figure 4.** Simulations carried out for systems of pristine and oxidized GNSs in water solvent. (a) PMF profiles for pristine and carboxylated GNSs and the contribution from water repulsion to the total PMFs. Points labeled by b, c, d, and e correspond to the parts b, c, d, and e, respectively. (b and c) Time-averaged normalized density profile and a snapshot of the simulation trajectory for pristine and carboxylated GNSs, respectively, at the specified COM distance. (d and e) TKE and displacement of a constraint free nanocarbon trapped in potential wells labeled as d and e on the PMF profiles of pristine and carboxylated GNSs, respectively, in part a, within a time span of 100 ps. Color scheme for the snapshots included in parts b and c: light blue, carbon; white, hydrogen; red, oxygen; and dark blue, water molecules.

attractions between the CNT carbon atoms, and the potential barrier hindering the nanocarbons falling into this trap (at a COM distance of 1.38 nm) is formed by the final layer of water molecules still confined between the CNTs. This strong barrier is attributed to the steric repulsions between the confined solvent molecules and the nanocarbons.[61] Figure 3b corresponds to the point b marked on Figure 3a and depicts the time-averaged normalized density (density profile normalized to bulk density of water) in conjunction with a snapshot of the simulation trajectory. As shown in this figure, water molecules are extremely packed (normalized density of ∼5) between the nanocarbons at this COM distance. This arises from the strong affinity of the water molecules for CNTs which are thermodynamically favored to be confined between them.[61] At a COM distance of 1.14 nm (Figure 3c), roughly all water molecules are desorbed and the CNTs are thoroughly adhered. Furthermore, Figure 3a indicates that for 1.4 nm < $d$ < 1.5 nm there is a strong water repulsion between the nanocarbons which stems from the final confined layer of water molecules visualized in Figure 3b, and for $d$ < 1.4 nm, where this confined layer has started to desorb, the water repulsion component stays at a constant level.

Figure 3a also demonstrates the PMF profiles for carboxylated and hydroxylated CNTs and water-induced repulsion component in these systems. In the previous section we discussed that the surface-modified nanocarbons are intrinsically less motivated to aggregate featuring a lower potential depth. A close look into the solvent-induced repulsion for pristine and oxidized nanocarbons in Figure 3a discloses a second important reason for the much higher stability of modified nanocarbons compared to the pristine ones; the solvent-induced repulsion is higher in the case of oxidized nanocarbons. Figure 3d and 3e reveals the reason for this observation. It is shown that the normalized density of water molecules is ∼2.5 and ∼1 at the points marked by d and e in Figure 3a, respectively, and consequently, one concludes that the functional groups enhance the confinement of the water molecules between nanocarbons. In other words, for the case of oxidized nanocarbons, the solvent molecules do not get totally desorbed since the functional attachments provide the water molecules with sufficient space between the basal carbon atoms, even at small COM distances at which the repulsive interactions between the functional atoms of one nanocarbon and the basal carbon atoms of the other one are operating.

Our studies revealed that three parameters play a crucial role in the stability of nanostructures in various solutions: (I) the height of the potential barrier against the nanostructures breakout from the deepest potential trap on the PMF profile (potential barrier height against dispersion, $\Delta H_D$, see Figure 3a), (II) the potential barrier height preventing the nanocarbons from getting stuck in the deepest potential trap (potential barrier height against aggregation, $\Delta H_A$, see Figure 3a), and (III) the translational kinetic energy (TKE) supplying the energy required to overcome an energy barrier which complements the two previously mentioned quantities. In fact, the information obtained from the PMF profiles, such as $\Delta H_D$ and $\Delta H_A$, provides valuable understanding of the aggregation and stability mechanisms but does not address some important


DOI: 10.1021/acs.jpcc.6b05318
J. Phys. Chem. C 2016, 120, 16804−16814

questions: are the nanocarbons capable of overcoming the barrier height against their aggregation if they are initially well dispersed? What is the approximate barrier height they can overcome at a specific temperature? What happens if they are stuck in a potential trap? Do they have any chance to get away or they will be restrained in the trap as long as there are no external stimuli, such as shaking, stirring, or sonication? We found the concept of translational kinetic energy (TKE) useful in addressing these questions and explaining the dispersion properties.

Figure 3f demonstrates the TKE and displacement of the free nanostructure (after removing the distance constraint) for a time span of 100 ps, corresponding to the point marked as f in Figure 3a. The average TKE of the pristine CNT trapped in this potential well is 1.19 kcal/mol, and the maximum TKE recorded in this time interval is 5.21 kcal/mol, while the nanocarbon is fluctuating in this potential well. Figure 3g depicts the same results for a carboxylated CNT trapped in the potential well labeled as g in Figure 3a. The average and maximum TKE recorded for this nanocarbon are 0.94 and 5.47 kcal/mol, respectively. The nanostructure in point c (for the pristine CNT) fluctuates at a higher frequency and a smaller interval compared to point g for the CNTCOOH since the former is stuck in a much tighter potential trap. Investigating the TKE and trajectories of these systems for a longer time span (~1 ns) showed that the maximum and average TKE stayed roughly the same as that in the first 100 ps. TKE of the nanostructure originates from two sources: the thermal energy and the energy obtained from the surrounding molecules through their collisions which is equivalent to the instantaneous forces whose time average forms the PMF profile. The pristine CNT trapped in the potential well f faces two highly steep walls, while the potential well for g is not as steep on one side. This explains the higher average TKE of the pristine CNT.

Figure 3a also reports the $\Delta H_D$ and $\Delta H_A$ for all three systems (in kcal/mol). For the case of CNTP, $\Delta H_D$ = 49.7 kcal/mol is extremely higher than the maximum TKE recorded here and we can conclude that a nanocarbon trapped in this deep potential well has a tiny chance to escape. For CNTCOOH, however, $\Delta H_D$ = 1.5 kcal/mol is lower than the maximum TKE and comparable to the average TKE, which results in a much higher escape probability. The nanostructure remains in the trap until it gains enough TKE in the proper direction to get out of it.

Considering an initially well-dispersed sample of carboxylated CNTs, if the nanocarbons get close and even become trapped at the deepest potential well on their PMF profiles they face a small barrier of 1.5 kcal/mol that can be provided by the thermal energy. However, this is not the case for pristine CNTs, which may require external stimuli to become dispersed again. This makes carboxylated CNTs much more stable in water in comparison to pristine CNTs. It should be noted that the value of $\Delta H_A$ for CNTP is higher than that of CNTCOOH (10.1 versus 6.6 kcal/mol); however, this does not make CNTP more stable than CNTCOOH in water as just discussed. In other words, all three parameters should be considered when evaluating the stability of nanostructures and comparing the stability of two different samples. The potential values for hydroxylated CNTs lie between those of pristine and carboxylated CNTs, and consequently, they must be more stable than pristine CNTs and less stable than the carboxylated ones.

The same simulations were carried out for systems of pristine and carboxylated graphene nanosheets in water solvent, and the results are presented in Figure 4. As inferred from Figure 4a, the difference between the solvent-induced repulsions of pristine and carboxylated nanocarbons is even higher in comparison to the case of CNT. Figure 4b and 4c shows that carboxylation enhances the solvent confinement to a high extent. In the case of pristine GNSs, the water molecules are totally desorbed at small COM distances, while for the carboxylated nanocarbons several water molecules with a normalized density of ~2.5 are still confined between the nanocarbons, giving rise to a high steric repulsion. Figure 4d and 4e reports the TKE and displacement of the GNSP and GNSCOOH initially placed in the situations marked as d and e, respectively, on Figure 4a. The maximum TKE is 8.22 kcal/mol for GNS and 5.93 kcal/mol for GNSCOOH. As in the case of CNT samples, the pristine nanocarbon trapped in a tighter potential well has an average TKE (1.31 kcal/mol) higher than that of the carboxylated GNS (1 kcal/mol) trapped in the e potential well. It is concluded from Figure 4a that carboxylated GNS has a higher $\Delta H_A$ (15.6 kcal/mol) than the pristine one (10.9 kcal/mol). However, as also discussed for the case of CNT, it is the much lower $\Delta H_D$ of the GNSCOOH compared to the GNSP (27.6 versus 240.7 kcal/mol) that makes it much more stable in water.

Next, In order to study the role of solvent type in the PMF profiles, we used DMF solvent. DMF is one of the most commonly used solvents for dispersing CNTs and exfoliating graphene sheets and provides the pristine nanocarbons with high stability.[12] Figure 5a and 5b depicts the PMF profiles

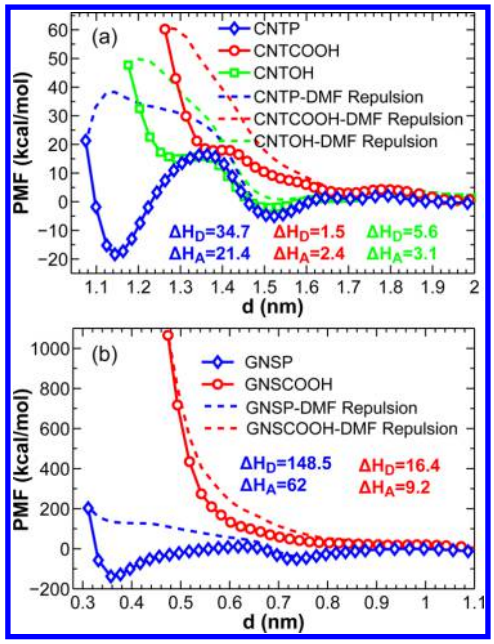


**Figure 5.** PMF profiles and their solvent-induced repulsion components for pristine and oxidized (a) CNTs and (b) GNSs in DMF solvent.

obtained for samples of pristine and oxidized CNTs and GNSs, respectively, in DMF. Also, monitoring the TKE of a nanocarbon in various points on the PMF profiles revealed that the maximum and average kinetic energy were in the same order as they were for the case of water solvent. As for the samples in water, oxidized nanocarbons, in DMF, have a much



DOI: 10.1021/acs.jpcc.6b05318
J. Phys. Chem. C 2016, 120, 16804−16814

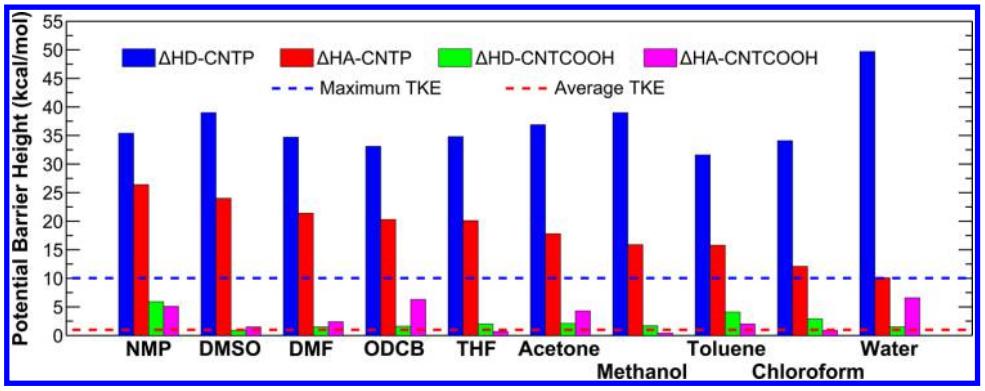


**Figure 6.** Potential barrier height against dispersion ($\Delta H_D$) and aggregation ($\Delta H_A$) for pristine and carboxylated CNTs in various solvents along with the typical level of the maximum and average TKE.

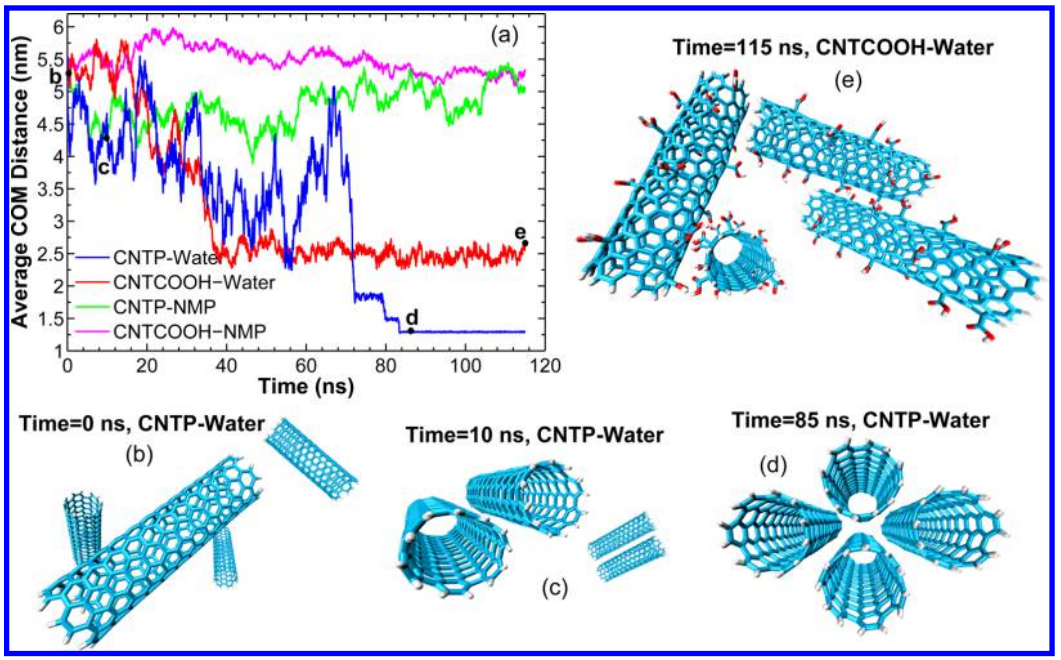


**Figure 7.** Free MD simulations for systems of pristine and carboxylated CNTs in water and NMP solvents. Each system contained four initially well-dispersed nanocarbons with random orientations and an initial average COM distance of ~5.4 nm. (a) Average COM distance of the four nanocarbons as a function of simulation time in a time span of 115 ns. Points labeled as b, c, d, and e correspond to the parts b, c, d, and e, respectively. (b) Initially well-dispersed configuration of the pristine CNTs in water solvent (other samples also had the same initial configuration). (c) Pairwise bundled configuration of the CNTP−water sample after 10 ns. (d) Thoroughly aggregated configuration of the CNTP−water sample after 85 ns into an energetically stable rhombic structure. (e) Final configuration of the CNTCOOH−water sample at 115 ns. Solvent molecules are not shown in the snapshots for more clarity. Color code: light blue, carbon; white, hydrogen; and red, oxygen.

stronger solvent-induced repulsion with respect to the pristine ones and are much more stable. From another point of view, the oxidized nanocarbons have lower $\Delta H_D$ values (in the order of the their kinetic energy) compared to the pristine nanocarbons, which makes them more stable in DMF.

Comparing the PMF profiles of pristine CNTs in Figures 3a and 5a in water and DMF respectively, one can conclude that DMF provides the pristine CNTs with a lower value of $\Delta H_D$ (34.7 versus 49.7 kcal/mol). However, in contrast to the way we previously compared the stability of pristine and oxidized nanocarbons in the same solvent considering their $\Delta H_D$ values, we suggest that it is the higher $\Delta H_A$ (21.4 versus 10.1 kcal/mol) of pristine CNTs in DMF compared to water that makes the former dispersion much more stable. In other words, overcoming a potential barrier of 34.7 kcal/mol for a pristine CNT which possesses a maximum and average TKE in the order of 10 and 1 kcal/mol, respectively, and is stuck in the deepest potential well in DMF can be as hard and unlikely as overcoming a potential barrier of 49.7 kcal/mol in water, without external stimuli. Consequently, considering a well-dispersed sample of pristine nanocarbons in DMF, the nanocarbons will face a high barrier ($\Delta H_A$) against their aggregation and will stay in the dispersed state, while for the pristine nanocarbons in water, they will have a low barrier ahead of them and will get aggregated more easily.

Figure 6, reporting the potential barrier heights, summarizes the information obtained from PMF profiles of the pristine and carboxylated CNTs in 10 solvents which are commonly used for dispersing CNTs and GNSs. In addition, monitoring the translational kinetic energies of pristine and carboxylated CNTs in various solvents showed that regardless of the solvent type and functionalization, at room temperature, the CNT nanostructures considered in this study have a maximum and average TKE in the order of 10 and 1 kcal/mol, respectively. As


DOI: 10.1021/acs.jpcc.6b05318
J. Phys. Chem. C 2016, 120, 16804−16814

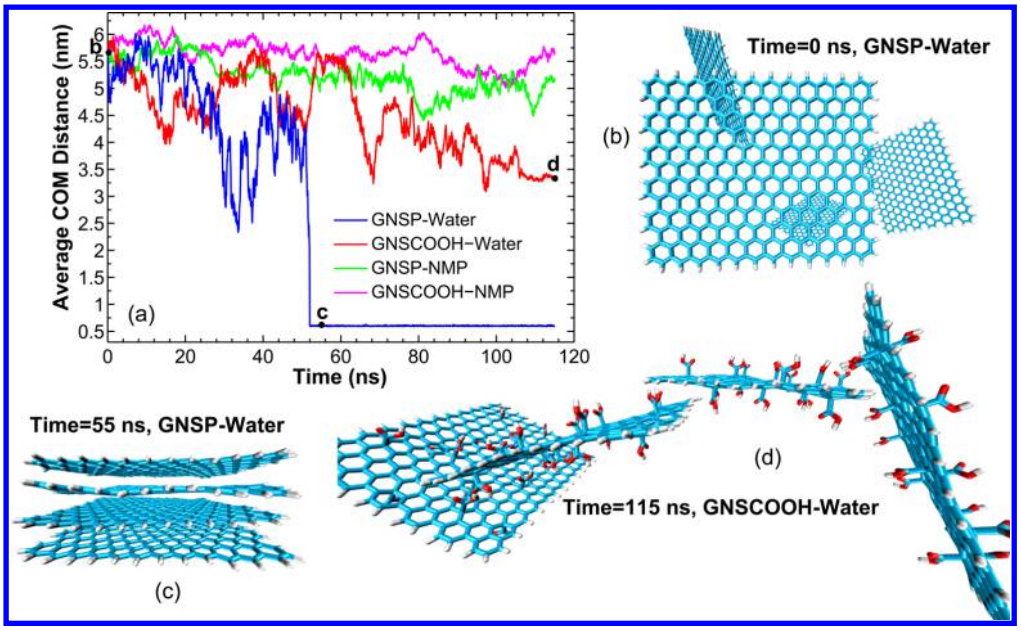


**Figure 8.** Free MD simulations for systems of pristine and carboxylated GNSs in water and NMP solvents. Each system contained four initially well-dispersed nanocarbons with random orientations and an initial average COM distance of ~5.6 nm. (a) Average COM distance of the four nanocarbons as a function of simulation time in a time span of 115 ns. Points labeled as b, c, and d correspond to parts b, c, and d, respectively. (b) Initially well-dispersed configuration of the pristine GNSs in water solvent (other samples also had the same initial configuration). (c) Totally stacked configuration of the GNSP−water sample after 55 ns. (d) Final configuration of the GNSCOOH−water sample at 115 ns. Solvent molecules are not shown in the snapshots for more clarity. Color code: light blue, carbon; white, hydrogen; and red, oxygen.

illustrated in Figure 6, for all solvents, carboxylated CNTs feature a much lower $\Delta H_D$ compared to the pristine CNTs. The $\Delta H_D$ values for carboxylated CNTs is lower than maximum TKE and in the order of the average TKE, while $\Delta H_D$ values for pristine nanocarbons are considerably higher than the maximum TKE. Accordingly and as discussed before, one can draw the conclusion that the carboxylated CNTs are much more stable than the pristine ones, in all solvents considered here, regardless of the fact that carboxylated CNTs possess a lower $\Delta H_A$ value in comparison with the pristine ones.

For comparing the ability of the solvents to disperse pristine CNTs, we note that the barrier height against dispersion ($\Delta H_D$) of pristine CNTs is substantially higher than the maximum TKE for all solvents, and we can conclude that if the pristine CNTs are bundled they will get severely restricted in the potential well. Consequently and as discussed before, one cannot use $\Delta H_D$ to compare the stability of pristine CNTs in different solvents. However, if we consider the $\Delta H_A$ values, we can conclude that for some solvents such as water and chloroform this value is in the order of the maximum TKE while for some others such as NMP and DMSO it is much higher than the maximum TKE. Considering pristine CNTs well dispersed in various solvents, the higher the barrier height they confront to aggregate ($\Delta H_A$) the lower their chance to succeed in doing so. Accordingly, we come to the conclusion that the ability of these solvents to disperse pristine CNTs is in the following order: NMP > DMSO > DMF > ODCB > THF > acetone > methanol > toluene > chloroform > water. This finding concurs with the results obtained by previous studies. For instance, Ausman et al.[62] suggested that pristine single-wall CNTs are more stable in NMP than in DMF on the basis of their UV−vis spectra. Liu et al.[41] did a more comprehensive job of comparing DMF, THF, toluene, and chloroform ability to disperse pristine multiwall CNTs. They found that the dispersions in DMF and THF were stable even 8 months after sonication, while in chloroform and toluene, bundles of CNTs were visible only 70 h after sonication. Also, employing the kinetic theory of colloid aggregation and PMF profiles, Shih et al.[61] predicted the ability of polar solvents to disperse pristine GNSs as NMP ≈ DMSO > DMF > water.

**Aggregation Process of Pristine and Oxidized Nanocarbons.** In the previous sections, we performed constrained MD simulations to obtain PMF profiles. In those simulations, two nanocarbons were constrained in different COM distances while they were restrained in a parallel configuration. In order to capture the details that were overlooked by the previous constrained simulations, we performed a set of larger scale, free MD simulations in this section. Each sample considered in the following studies contained four initially well-dispersed and randomly oriented nanocarbons in a relatively large simulation box of ~12 × 12 × 12 $nm^3$ filled with thousands of solvent molecules.

Figure 7 presents the results of the free MD simulations for samples of pristine and carboxylated CNTs in water and NMP solvents. The average COM distance of the four nanocarbons is plotted as a function of simulation time in a span of 115 ns in Figure 7a. In addition, Figure 7b−e demonstrates snapshots of the simulation trajectories at various moments in water, leaving out the solvent molecules for clarity. All four samples were initially prepared in the well-dispersed, randomly oriented configuration demonstrated in Figure 7b. As depicted in Figure 7a and in contrast to the samples in water, the dispersions of the both pristine and carboxylated CNTs were stable in NMP, and these samples did not get aggregated until the end of the simulation time. The average COM distance in the case of carboxylated CNTs in NMP was even higher than that for the pristine ones.

For pristine CNTs in water it was observed that the nanocarbons freely diffused until they randomly touched. Then


DOI: 10.1021/acs.jpcc.6b05318
J. Phys. Chem. C 2016, 120, 16804−16814

their interface grew and they got aligned and finally coalesced. The nanocarbons quickly aggregated into the pairwisely bundled configuration visualized in Figure 7c, and after ∼83 ns they got totally bundled into the rhombic, energetically favorable structure depicted in Figure 7d. This behavior is also reflected in the average COM distance in Figure 7a. An interesting observation was that the carboxylated CNTs locally aggregated in water but did not get bundled as the pristine CNTs did (see the final configuration of the carboxylated CNTs in water in Figure 7e). This local aggregation occurred at areas which were bare of functional groups and is accountable for the lower average COM distance of the carboxylated CNTs in water compared to those of NMP dispersions. As the CNTs, in practice, are several orders of magnitude longer than the ones simulated here, this effect may not be as observable as it is here.

The aggregation behavior of GNSs was also studied through free MD simulations, and the results are depicted in Figure 8. Figure 8a plots the average COM distances of the pristine and carboxylated nanocarbons in water and NMP solvents which were initially dispersed to the configuration illustrated in Figure 8b. As in the case of CNT, the dispersions of pristine and carboxylated GNSs were stable in NMP. The pristine GNSs were extremely unstable in water and formed the stacked structure visualized in Figure 8c after ∼55 ns. Also, the carboxylated GNSs got locally aggregated at functional group-bare areas and formed the configuration depicted in Figure 8d at the end of simulation.

As discussed above, the carboxylated nanocarbons can get locally aggregated in the areas which are bare of functional groups. Accordingly, the ability of a solvent to disperse carboxylated nanocarbons is not independent of its ability to disperse pristine nanocarbons. On this account, we can conclude that the solvent capability of dispersing oxidized nanocarbons follows the same rating mentioned for the case of pristine ones. This claim is also consistent with experimental observations. For example, Tchoul et al.[31] showed that nitric acid-treated single-wall CNTs are more dispersible in DMF than they are in methanol and water.

## CONCLUSION

We performed large-scale all-atom molecular dynamic simulations in order to study the dispersion properties and aggregation kinetics of pristine and oxidized single-wall CNTs and single-layer GNSs in 10 various, commonly used solvents. Potential of mean force profiles were calculated for this purpose through constrained MD simulations. We also complemented the information obtained from PMF profiles utilizing the concept of translational kinetic energy. Three parameters should be taken into account when deciding the stability of nanostructures in solvent media. These include the barrier height against dispersion ($\Delta H_D$) and aggregation ($\Delta H_A$), which are obtained from PMF curves, as well as the maximum and average kinetic energy of the nanocarbons.

The results revealed the important facts leading to the much more stable dispersions of oxidized nanocarbons than those of pristine ones in the polar solvents. The nanocarbons bearing functional groups such as carboxyl and hydroxyl groups are less motivated to aggregate. Also, the solvent-induced repulsion is higher for the case of oxidized nanocarbons. This originates from the fact that the functional groups promote the confinement of solvent molecules between the nanocarbons. It was observed that for carboxylated nanocarbons the solvent molecules do not desorb even at small COM distances where the inherent repulsive forces are in operation. The much higher stability of oxidized nanocarbons can also be explained regarding the fact that they have a much lower $\Delta H_D$, which is in the order of their TKE. As a consequence, they can easily flee the potential traps even if they get stuck.

The ability of various polar solvents to disperse pristine nanocarbons was ranked as NMP > DMSO > DMF > ODCB > THF > acetone > methanol > toluene > chloroform > water. For pristine nanocarbons which have high $\Delta H_D$ values, it was concluded that the samples with higher $\Delta H_A$ are more stable. In addition, free MD simulations showed that the carboxylated nanocarbons in inefficient solvents are prone to locally aggregate in areas without functional atoms. This led us to the conclusion that the same solvent ranking applies to the case of oxidized nanocarbons as well.

## ASSOCIATED CONTENT

### Supporting Information

The Supporting Information is available free of charge on the ACS Publications website at DOI: 10.1021/acs.jpcc.6b05318.

Discussion on the partial charge calculation for pristine and oxidized nanocarbons; detailed partial charge information obtained from the DFT calculations for DMF, THF, NMP, chloroform, and toluene molecules as well as the partial charges taken from the OPLS-AA force field for acetone, methanol, DMSO, and ODCB molecules; sample structures used to calculate the partial charges of carboxyl and hydroxyl functional atoms attached to a carbon nanostructure; partial charges of the functional groups obtained utilizing the B3LYP/6-311++G** theory (PDF)

## AUTHOR INFORMATION

### Corresponding Author

*Tel: +98-21-6111-4982, Fax: +98-21-8801-3199 E-mail: pourfath@ut.ac.ir;pourfath@iue.tuwien.ac.at.

### Notes

The authors declare no competing financial interest.

## ACKNOWLEDGMENTS

This work was partially funded by Iran National Science Foundation (INSF). Also, the computational results presented have been achieved using the Vienna Scientific Cluster (VSC).

## REFERENCES

(1) Hu, L.; Hecht, D. S.; Gruner, G. Carbon Nanotube Thin Films: Fabrication, Properties, and Applications. *Chem. Rev.* **2010**, *110*, 5790−5844.

(2) Avouris, P.; Chen, Z.; Perebeinos, V. Carbon-Based Electronics. *Nat. Nanotechnol.* **2007**, *2*, 605−615.

(3) Liu, Y.; Dong, X.; Chen, P. Biological and Chemical Sensors Based on Graphene Materials. *Chem. Soc. Rev.* **2012**, *41*, 2283−2307.

(4) Volder, M. F. L. D.; Tawfick, S. H.; Baughman, R. H.; Hart, A. J. Carbon Nanotubes: Present and Future Commercial Applications. *Science* **2013**, *339*, 535−539.

(5) Baughman, R. H.; Zakhidov, A. A.; de Heer, W. A. Carbon Nanotubes-the Route Toward Applications. *Science* **2002**, *297*, 787−792.

(6) Azar, N. S.; Pourfath, M. A Comprehensive Study of Transistors Based on Conductive Polymer Matrix Composites. *IEEE Trans. Electron Devices* **2015**, *62*, 1584−1589.



DOI: 10.1021/acs.jpcc.6b05318
J. Phys. Chem. C 2016, 120, 16804−16814

(7) Ramanathan, T.; Abdala, A. A.; Stankovich, S.; Dikin, D. A.; Herrera-Alonso, M.; Piner, R. D.; Adamson, D. H.; Schniepp, H. C.; Chen, X.; Ruoff, R. S.; et al. Functionalized Graphene Sheets for Polymer Nanocomposites. *Nat. Nanotechnol.* **2008**, *3*, 327−331.
(8) Zhang, Y.; Sheehan, C. J.; Zhai, J.; Zou, G.; Luo, H.; Xiong, J.; Zhu, Y. T.; Jia, Q. X. Polymer-Embedded Carbon Nanotube Ribbons for Stretchable Conductors. *Adv. Mater.* **2010**, *22*, 3027−3031.
(9) Stankovich, S.; Dikin, D. A.; Dommett, G. H.; Kohlhaas, K. M.; Zimney, E. J.; Stach, E. A.; Piner, R. D.; Nguyen, S. T.; Ruoff, R. S. Graphene-Based Composite Materials. *Nature* **2006**, *442*, 282−286.
(10) Hsiao, S.-T.; Ma, C.-C. M.; Tien, H.-W.; Liao, W.-H.; Wang, Y.-S.; Li, S.-M.; Yang, C.-Y.; Lin, S.-C.; Yang, R.-B. Effect of Covalent Modification of Graphene Nanosheets on the Electrical Property and Electromagnetic Interference Shielding Performance of a Water-Borne Polyurethane Composite. *ACS Appl. Mater. Interfaces* **2015**, *7*, 2817−2826.
(11) Yousefi, N.; Sun, X.; Lin, X.; Shen, X.; Jia, J.; Zhang, B.; Tang, B.; Chan, M.; Kim, J. Highly Aligned Graphene/Polymer Nanocomposites with Excellent Dielectric Properties for High-Performance Electromagnetic Interference Shielding. *Adv. Mater.* **2014**, *26*, 5480−5487.
(12) Yan, L.; Zheng, Y. B.; Zhao, F.; Li, S.; Gao, X.; Xu, B.; Weiss, P. S.; Zhao, Y. Chemistry and Physics of a Single Atomic Layer: Strategies and Challenges for Functionalization of Graphene and Graphene-Based Materials. *Chem. Soc. Rev.* **2012**, *41*, 97−114.
(13) Hudson, J. L.; Casavant, M. J.; Tour, J. M. Water-Soluble, Exfoliated, Nonroping Single-Wall Carbon Nanotubes. *J. Am. Chem. Soc.* **2004**, *126*, 11158−11159.
(14) Li, D.; Mueller, M. B.; Gilje, S.; Kaner, R. B.; Wallace, G. G. Processable Aqueous Dispersions of Graphene Nanosheets. *Nat. Nanotechnol.* **2008**, *3*, 101−105.
(15) Chen, J.; Hamon, M. A.; Hu, H.; Chen, Y.; Rao, A. M.; Eklund, P. C.; Haddon, R. C. Solution Properties of Single-Walled Carbon Nanotubes. *Science* **1998**, *282*, 95−98.
(16) An, X.; Simmons, T.; Shah, R.; Wolfe, C.; Lewis, K. M.; Washington, M.; Nayak, S. K.; Talapatra, S.; Kar, S. Stable Aqueous Dispersions of Noncovalently Functionalized Graphene from Graphite and Their Multifunctional High-Performance Applications. *Nano Lett.* **2010**, *10*, 4295−4301.
(17) Islam, M. F.; Rojas, E.; Bergey, D. M.; Johnson, A. T.; Yodh, A. G. High Weight Fraction Surfactant Solubilization of Single-Wall Carbon Nanotubes in Water. *Nano Lett.* **2003**, *3*, 269−273.
(18) Sturzl, N.; Hennrich, F.; Lebedkin, S.; Kappes, M. M. Near Monochiral Single-Walled Carbon Nanotube Dispersions in Organic Solvents. *J. Phys. Chem. C* **2009**, *113*, 14628−14632.
(19) Worsley, K. A.; Kalinina, I.; Bekyarova, E.; Haddon, R. C. Functionalization and Dissolution of Nitric Acid Treated Single-Walled Carbon Nanotubes. *J. Am. Chem. Soc.* **2009**, *131*, 18153−18158.
(20) Gulotty, R.; Castellino, M.; Jagdale, P.; Tagliaferro, A.; Balandin, A. A. Effects of Functionalization on Thermal Properties of Single-Wall and Multi-Wall Carbon Nanotube-Polymer Nanocomposites. *ACS Nano* **2013**, *7*, 5114−5121.
(21) Peng, H.; Alemany, L. B.; Margrave, J. L.; Khabashesku, V. N. Sidewall Carboxylic Acid Functionalization of Single-Walled Carbon Nanotubes. *J. Am. Chem. Soc.* **2003**, *125*, 15174−15182.
(22) Wang, Y.; Iqbal, Z.; Mitra, S. Rapidly Functionalized, Water-Dispersed Carbon Nanotubes at High Concentration. *J. Am. Chem. Soc.* **2006**, *128*, 95−99.
(23) Liu, J.; Rinzler, A. G.; Dai, H.; Hafner, J. H.; Bradley, R. K.; Boul, P. J.; Lu, A.; Iverson, T.; Shelimov, K.; Huffman, C. B.; et al. Fullerene Pipes. *Science* **1998**, *280*, 1253−1256.
(24) Yu, H.; Jin, Y.; Peng, F.; Wang, H.; Yang, J. Kinetically Controlled Side-Wall Functionalization of Carbon Nanotubes by Nitric Acid Oxidation. *J. Phys. Chem. C* **2008**, *112*, 6758−6763.
(25) Romanos, G. E.; Likodimos, V.; Marques, R. R.; Steriotis, T. A.; Papageorgiou, S. K.; Faria, J. L.; Figueiredo, J. L.; Silva, A. M.; Falaras, P. Controlling and Quantifying Oxygen Functionalities on Hydrothermally and Thermally Treated Single-Wall Carbon Nanotubes. *J. Phys. Chem. C* **2011**, *115*, 8534−8546.
(26) Kundu, S.; Wang, Y.; Xia, W.; Muhler, M. Thermal Stability and Reducibility of Oxygen-Containing Functional Groups on Multiwalled Carbon Nanotube Surfaces: A Quantitative High-Resolution XPS and TPD/TPR Study. *J. Phys. Chem. C* **2008**, *112*, 16869−16878.
(27) Zhang, G.; Sun, S.; Yang, D.; Dodelet, J.-P.; Sacher, E. The Surface Analytical Characterization of Carbon Fibers Functionalized by H2SO4/HNO3 Treatment. *Carbon* **2008**, *46*, 196−205.
(28) Heister, E.; Lamprecht, C.; Neves, V.; Tilmaciu, C.; Datas, L.; Flahaut, E.; Soula, B.; Hinterdorfer, P.; Coley, H. M.; Silva, S. R. P.; et al. Higher Dispersion Efficacy of Functionalized Carbon Nanotubes in Chemical and Biological Environments. *ACS Nano* **2010**, *4*, 2615−2626.
(29) Bergeret, C.; Cousseau, J.; Fernandez, V.; Mevellec, J.-Y.; Lefrant, S. Spectroscopic Evidence of Carbon Nanotubes' Metallic Character Loss Induced by Covalent Functionalization via Nitric Acid Purification. *J. Phys. Chem. C* **2008**, *112*, 16411−16416.
(30) Del Canto, E.; Flavin, K.; Movia, D.; Navio, C.; Bittencourt, C.; Giordani, S. Critical Investigation of Defect Site Functionalization on Single-Walled Carbon Nanotubes. *Chem. Mater.* **2011**, *23*, 67−74.
(31) Tchoul, M. N.; Ford, W. T.; Lolli, G.; Resasco, D. E.; Arepalli, S. Effect of Mild Nitric Acid Oxidation on Dispersability, Size, and Structure of Single-Walled Carbon Nanotubes. *Chem. Mater.* **2007**, *19*, 5765−5772.
(32) Shih, C.-J.; Lin, S.; Strano, M. S.; Blankschtein, D. Understanding the Stabilization of Single-Walled Carbon Nanotubes and Graphene in Ionic Surfactant Aqueous Solutions: Large-Scale Coarse-Grained Molecular Dynamics Simulation-Assisted DLVO Theory. *J. Phys. Chem. C* **2015**, *119*, 1047−1060.
(33) Suttipong, M.; Tummala, N. R.; Kitiyanan, B.; Striolo, A. Role of Surfactant Molecular Structure on Self-Assembly: Aqueous SDBS on Carbon Nanotubes. *J. Phys. Chem. C* **2011**, *115*, 17286−17296.
(34) Tummala, N. R.; Striolo, A. Role of Counterion Condensation in the Self-Assembly of SDS Surfactants at the Water-Graphite Interface. *J. Phys. Chem. B* **2008**, *112*, 1987−2000.
(35) Xu, Z.; Yang, X.; Yang, Z. A Molecular Simulation Probing of Structure and Interaction for Supramolecular Sodium Dodecyl Sulfate/Single-Wall Carbon Nanotube Assemblies. *Nano Lett.* **2010**, *10*, 985−991.
(36) Lin, S.; Shih, C.-J.; Strano, M. S.; Blankschtein, D. Molecular Insights into the Surface Morphology, Layering Structure, and Aggregation Kinetics of Surfactant-Stabilized Graphene Dispersions. *J. Am. Chem. Soc.* **2011**, *133*, 12810−12823.
(37) Choudhury, N.; Pettitt, B. M. On the Mechanism of Hydrophobic Association of Nanoscopic Solutes. *J. Am. Chem. Soc.* **2005**, *127*, 3556−3567.
(38) Zhang, Z.; Turner, C. H. Water-Induced Interactions Between Boron-Doped Carbon Nanotubes. *J. Phys. Chem. C* **2014**, *118*, 17838−17846.
(39) Cao, Z.; Peng, Y.; Li, S.; Liu, L.; Yan, T. Molecular Dynamics Simulation of Fullerene $C_{60}$ in Ethanol Solution. *J. Phys. Chem. C* **2009**, *113*, 3096−3104.
(40) Angelikopoulos, P.; Bock, H. The Nanoscale Cinderella Problem: Design of Surfactant Coatings for Carbon Nanotubes. *J. Phys. Chem. Lett.* **2011**, *2*, 139−144.
(41) Liu, C.-X.; Choi, J.-W. Improved Dispersion of Carbon Nanotubes in Polymers at High Concentrations. *Nanomaterials* **2012**, *2*, 329−347.
(42) Jorgensen, W. L.; Maxwell, D. S.; Tirado-Rives, J. Development and Testing of the OPLS All-Atom Force Field on Conformational Energetics and Properties of Organic Liquids. *J. Am. Chem. Soc.* **1996**, *118*, 11225−11236.
(43) Kaminski, G. A.; Friesner, R. A.; Tirado-Rives, J.; Jorgensen, W. L. Evaluation and Reparametrization of the OPLS-AA Force Field for Proteins via Comparison with Accurate Quantum Chemical Calculations on Peptides. *J. Phys. Chem. B* **2001**, *105*, 6474−6487.
(44) Berendsen, H. J. C.; Grigera, J. R.; Straatsma, T. P. The Missing Term in Effective Pair Potentials. *J. Phys. Chem.* **1987**, *91*, 6269−6271.


DOI: 10.1021/acs.jpcc.6b05318
J. Phys. Chem. C 2016, 120, 16804−16814

(45) Valiev, M.; Bylaska, E. J.; Govind, N.; Kowalski, K.; Straatsma, T. P.; Van Dam, H. J. J.; Wang, D.; Nieplocha, J.; Apra, E.; Windus, T.; et al. NWChem: a Comprehensive and Scalable Open-Source Solution for Large Scale Molecular Simulations. *Comput. Phys. Commun.* **2010**, *181*, 1477−1489.
(46) Lide, D. R. *CRC Handbook of Chemistry and Physics*; CRC Press: Boca Raton, FL, 2005.
(47) Elstner, M.; Porezag, D.; Jungnickel, G.; Elsner, J.; Haugk, M.; Frauenheim, T.; Suhai, S.; Seifert, G. Self-Consistent-Charge Density-Functional Tight-Binding Method for Simulations of Complex Materials Properties. *Phys. Rev. B: Condens. Matter Mater. Phys.* **1998**, *58*, 7260−7268.
(48) Aradi, B.; Hourahine, B.; Frauenheim, T. DFTB+, a Sparse Matrix-Based Implementation of the DFTB Method. *J. Phys. Chem. A* **2007**, *111*, 5678−5684.
(49) Saikia, N.; Jha, A. N.; Deka, R. C. Dynamics of Fullerene-Mediated Heat-Driven Release of Drug Molecules from Carbon Nanotubes. *J. Phys. Chem. Lett.* **2013**, *4*, 4126−4132.
(50) Hummer, G.; Rasaiah, J. C.; Noworyta, J. P. Water Conduction Through the Hydrophobic Channel of a Carbon Nanotube. *Nature* **2001**, *414*, 188−190.
(51) Huang, L.-L.; Shao, Q.; Lu, L.-H.; Lu, X.-H.; Zhang, L.-Z.; Wang, J.; Jiang, S.-y. Helicity and Temperature Effects on Static Properties of Water Molecules Confined in Modified Carbon Nanotubes. *Phys. Chem. Chem. Phys.* **2006**, *8*, 3836−3844.
(52) Balamurugan, K.; Baskar, P.; Kumar, R. M.; Das, S.; Subramanian, V. Effects of Functionalization of Carbon Nanotubes on Their Dispersion in an Ethylene Glycol-Water Binary Mixture-a Molecular Dynamics and ONIOM Investigation. *Phys. Chem. Chem. Phys.* **2014**, *16*, 24509−24518.
(53) Van Der Spoel, D.; Lindahl, E.; Hess, B.; Groenhof, G.; Mark, A. E.; Berendsen, H. J. GROMACS: Fast, Flexible, and Free. *J. Comput. Chem.* **2005**, *26*, 1701−1718.
(54) Hess, B.; Kutzner, C.; van der Spoel, D.; Lindahl, E. GROMACS 4: Algorithms for Highly Efficient, Load-Balanced, and Scalable Molecular Simulation. *J. Chem. Theory Comput.* **2008**, *4*, 435−447.
(55) Parrinello, M.; Rahman, A. Polymorphic Transitions in Single Crystals: A New Molecular Dynamics Method. *J. Appl. Phys.* **1981**, *52*, 7182−7190.
(56) Hoover, W. G. Canonical Dynamics: Equilibrium Phase-Space Distributions. *Phys. Rev. A: At., Mol., Opt. Phys.* **1985**, *31*, 1695−1697.
(57) Berendsen, H. J.; van Postma, J.; van Gunsteren, W. F.; DiNola, A. R. H. J.; Haak, J. R. Molecular Dynamics with Coupling to an External Bath. *J. Chem. Phys.* **1984**, *81*, 3684−3690.
(58) Darden, T.; York, D.; Pedersen, L. Particle Mesh Ewald: An *N.log*(*N*) Method for Ewald Sums in Large Systems. *J. Chem. Phys.* **1993**, *98*, 10089−10092.
(59) Hess, B.; Bekker, H.; Berendsen, H. J.; Fraaije, J. G. LINCS: A Linear Constraint Solver for Molecular Simulations. *J. Comput. Chem.* **1997**, *18*, 1463−1472.
(60) Tang, L.; Yang, X. Molecular Dynamics Simulation of $C_{60}$ Encapsulation into Single-Walled Carbon Nanotube in Solvent Conditions. *J. Phys. Chem. C* **2012**, *116*, 11783−11791.
(61) Shih, C.-J.; Lin, S.; Strano, M. S.; Blankschtein, D. Understanding the Stabilization of Liquid-Phase-Exfoliated Graphene in Polar Solvents: Molecular Dynamics Simulations and Kinetic Theory of Colloid Aggregation. *J. Am. Chem. Soc.* **2010**, *132*, 14638−14648.
(62) Ausman, K. D.; Piner, R.; Lourie, O.; Ruoff, R. S.; Korobov, M. Organic Solvent Dispersions of Single-Walled Carbon Nanotubes: Toward Solutions of Pristine Nanotubes. *J. Phys. Chem. B* **2000**, *104*, 8911−8915.


DOI: 10.1021/acs.jpcc.6b05318
*J. Phys. Chem. C* 2016, 120, 16804−16814